



Sensitivity analysis for airborne sounding of the troposphere by GNSS radio occultation

O. Lesne^a, J. Haase^{a,*}, G. Kirchengast^b, J. Ramsauer^b, W. Poetzi^b

^a ACRI-ST, Sophia-Antipolis, France

^b IGAMI/University of Graz, Austria

Accepted 12 January 2002

Abstract

The usual geometry for radio occultation sounding using global navigation satellite system (GNSS) signals has the receiver placed on a low earth orbit (LEO) satellite. We investigate a new geometric approach, assuming an airborne rather than a spaceborne receiver. Information on the refractivity structure and hence the pressure, temperature, and humidity can be retrieved from accurate airborne measurements of amplitude and phase delay of the signals occulted by the troposphere. We present some advantages and disadvantages for the concept of making measurements from commercial aircraft equipped with proper GNSS receivers and antennae compared to the spaceborne case. We simulated realistic airborne occultation observations and assessed the characteristics of their geometry and sampling. We also compared the dynamic range of the signal with the magnitude of error sources that affect the measurements. Findings include that an airborne system has the potential to provide more profiles per unit area below 10 km height than a constellation of up to 25 satellites over the North Atlantic (though with inferior global coverage), and that the signal to noise ratio (SNR) should be better below 5 km than in the LEO case. Though the receiver velocity error is larger than for the LEO system, it is still small enough relative to the signal level to retrieve useful information. The estimated sensitivity of the technique is better than 0.1% refractivity at 3 km altitude increasing to 0.5% refractivity at 11 km. Because of the large horizontal drift of the tangent point of up to 450 km, the assumption of spherical symmetry in the existence of significant 3D variations in structure is expected to be a major error source, in addition to the airplane velocity uncertainty. © 2002 Published by Elsevier Science Ltd.

1. Introduction

Radio occultation is a technique for sounding the atmosphere using radio or microwave signals recorded at a moving receiver as it sets (or rises from) behind the horizon. In our study the transmitter is one of a constellation of global navigation system satellites (GNSS) transmitting at microwave frequencies and the receiver is on an airborne platform such as a long haul commercial aircraft. As the GNSS satellite sets, the ray path samples successively deeper into the atmosphere. The ray path is refracted and the carrier phase signal is delayed because of the increase in refractivity with decreasing altitude. Information on the temperature and humidity of the atmosphere can then be retrieved from the derived refractivity. The technique was first used on

planetary atmospheres (e.g., Fjeldbo et al., 1971) then proposed for studying Earth's atmosphere by using a receiver on a LEO satellite (Melbourne et al., 1994) and tested on the GPS/MET "proof-of-concept" mission (Ware et al., 1996; Rocken et al., 1997). Current missions providing radio occultation soundings include the CHAMP mission (Wickert et al., 2001) and the SAC-C mission. The technique was recently proposed for mountain-top receivers (Zuffada et al., 1999), which share characteristics with the airborne case, but are not affected by noise sources such as uncertainties in receiver motion. The authors suggested that the technique could be applied to airborne receivers.

This paper describes a preliminary investigation of the characteristics, the signal dynamics and the effects of error sources such as the airplane position and velocity uncertainty on refractivity. We use a forward modeling approach to calculate the change in the phase delay due to perturbations of the input refractivity model. We then compare the difference in the phase delays to the magnitude of the noise sources. This provides an estimate of

* Corresponding author. Present address: Department of Earth and Atmospheric Science, Purdue University, West Lafayette, IN 47907-1397, USA. Tel.: +1-765-494-1643; fax: +1-765-496-1210/+33-4-93-95-80-98.

E-mail address: jhaase@purdue.edu (J. Haase).

the sensitivity of the technique given a threshold error level.

1.1. EGOPS simulations

The software tool used in this study was the end-to-end GNSS occultation performance simulator (EGOPS), Version 4 α . It was designed for observation simulation and analysis of the capabilities of the GPS/GLONASS GNSS radio occultation technique for measuring temperature and water vapor of Earth's atmosphere (Kirchengast, 1998; Kirchengast et al., 2001; Ramsauer and Kirchengast, 2000). It supports mission analysis/planning, generation of simulated atmospheric profiling observations, and evaluation of the quality of measurements obtained with a given scenario.

The 3D ray tracing algorithm (Hoeg et al., 1995) used for computing the excess phase of the carrier wave signal is based on the 3D Haselgrove equations in Cartesian coordinates. The equations are solved using a predictor–corrector method with adaptive step size started by a fourth-order Runge–Kutta algorithm. The ray paths connecting the specified airplane positions to the specified GNSS positions are found using a shooting method with an iterative Newton–Raphson method of finding roots in three dimensions. The output of EGOPS is the simulated signal excess phase and amplitude for a given occultation geometry as a function of time. The excess phase already has the straight line distance subtracted.

1.2. Methodology for tests

EGOPS does not currently have the functionality to carry out retrievals for refractivity and other atmospheric properties for the airborne case. Thus it is not possible to introduce errors into the simulated data and see their effect on the retrieved profiles. Our approach in all the following simulations is therefore to introduce some perturbations into the input atmospheric model and compare the difference in the simulated observations with the size of the error sources. The objective is to give an order of magnitude estimate of the sensitivity of the system to the different instrumental error sources.

The excess Doppler shift as well as the bending angle are calculated in two modules exterior to EGOPS. The excess Doppler shift is calculated by taking the time derivative of the excess phase 1 Hz output and smoothing over five consecutive time points. It is also mapped to the tangent point altitude before comparison with other profiles. This mapping is important because of the large variations in the time duration of the profile due to the geometry of the occultations. The second module transforms the excess Doppler to bending angle by taking as input the excess Doppler profile and the EGOPS output velocities and positions for the transmitter and receiver. Because of atmo-

spheric bending, the Doppler shift is different than the one expected due to the projection of the receiver and transmitter velocity on the straight line direction. This atmospheric bending angle is calculated based on the equations developed for the LEO case (Vorobev and Krasil'nikova, 1994).

2. Geometric simulations of the spatial sampling

These simulations address the expected sampling of an airborne observational system taking into account a realistic flight schedule such as that used for the aircraft meteorological data reporting (AMDAR) system. AMDAR is an initiative for reporting measurements of temperature, pressure, and other meteorological parameters on commercial airline flights for use in numerical weather prediction (EUCOS, 1997). The first objective here is to investigate the horizontal sampling so as to get an idea on the number and distribution of occultation profiles which could be obtained if all the aircrafts used for AMDAR observations were equipped with GPS receivers and antennae sufficiently accurate for radio occultation.

Based on the aircraft positions from an AMDAR data file from 18 October 2000 containing all European AMDAR flights and meteorological data, we simulated the occultations that would occur based on the GPS constellation ephemeris for that day which contained 26 satellites. The AMDAR file contains the coordinates of the airplane during its ascent and descent phase every 30 s and every 7 min during level flight. The aircraft fly at a very limited range of speeds and altitudes. We chose the representative speed of 900 km/h and altitude of 11 km for the simulations. Fig. 1 shows the 312 flights extracted from the AMDAR file whose latitude and longitude difference between begin and end points of the flight is more than 1.5°. For some flights, there are gaps in the data which lead to a lower number of occultations calculated with EGOPS than one could expect in reality. Nevertheless the number of gaps is relatively small and the simulation gives a representative distribution.

With 312 long flights, we obtained 998 occultations over Europe with a high density of profiles above France, to some extent due to the large contribution to the data set from major European carriers based in the UK and France. Fourteen AMDAR aircrafts were flying over the Atlantic ocean on this day, providing a total of about 225 occultations. Sampling of this region is of great importance for prediction of weather in Europe (EUCOS, 1997). This number is much greater than the number of occultations over the North Atlantic produced by a single LEO spacecraft equipped with a GPS receiver, where we calculated the number of occultations per day to be about 8 in a typical EGOPS simulation.

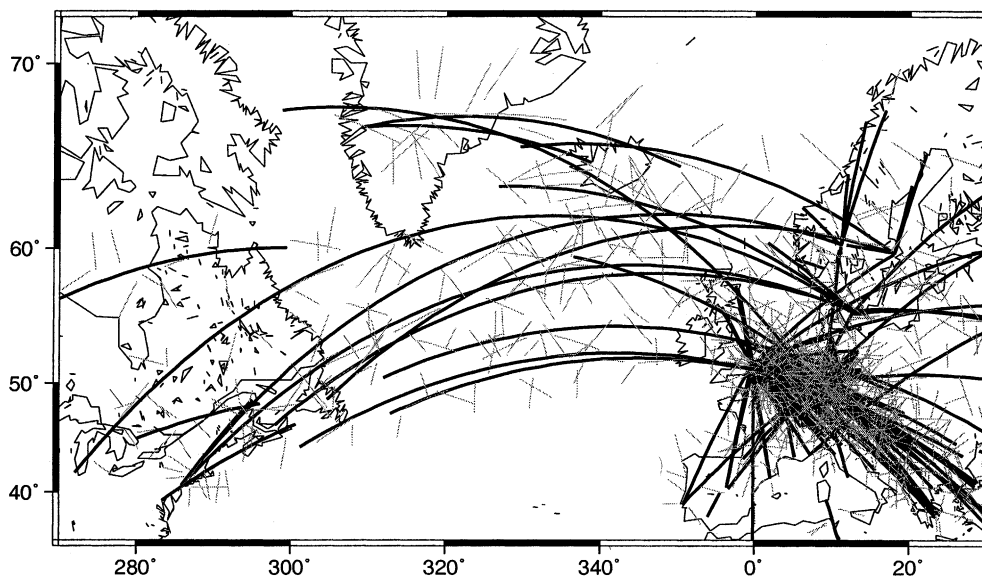


Fig. 1. 312 Long distance flights which reported AMDAR data for one day (October 18, 2000; dark lines) and the resulting occultation profiles (grey lines) over the Atlantic ocean. Linear extent of profiles indicates approximate drift of tangent point over the duration of the occultation.

Even with a constellation of 25 satellites the spatial sampling would not be as dense in the region covered by flight trajectories (about 200 occultations). Of course, the airborne occultation profiles do not provide global coverage and do not extend as high into the atmosphere as in the LEO case.

The geometry of a single occultation is significantly different for an airborne as opposed to a LEO occultation. Because of the much lower receiver velocity, the duration of the occultation is determined primarily by the time it takes for the GNSS satellite to set or rise. In the case of the LEO, the duration of the occultation is determined by the setting or rising of the LEO satellite, thus the occultations are much shorter, on the order of 30 s for the lowest 10 km of a LEO occultation versus about 9 min for an airborne occultation. In addition, since the GNSS satellite is generally traversing a large azimuthal range of the visible sky, and because the aircraft velocity is so much lower than the GNSS velocity, there is a significant horizontal drift of the tangent point over the course of an airborne occultation. The horizontal drift varies from about 200 to 470 km, as opposed to a typical drift of about 50 to 200 km for LEO occultations.

3. Signal dynamics simulations

These simulations are aimed at estimating the expected phase and amplitude variations and Doppler shift dynamics for an airborne occultation using a standard 1D atmosphere and comparing them to the equivalent occultation geometry for the case of a receiver on a LEO platform.

3.1. Airplane case

The reference case uses a 1D bi-exponential atmosphere based on two scale heights, one for the dry atmosphere (about 7 km) and a smaller scale height (2 km) for the moist atmosphere (Ramsauer and Kirchengast, 2000). We simulate an occultation occurring during a Paris–New York flight (see Fig. 2) in the middle of the Atlantic. The simulation was computed without including effects of the ionosphere, assuming that these delays could be removed with negligible error using dual frequency measurements. This setting occultation has a typical oblique geometry where the tangent point profile has an azimuth of -96° with respect to the airplane trajectory.

The occultation for the airplane case lasts 8 min 4 s and the horizontal drift of the tangent point is ~ 260 km. Results plotted in Fig. 3 (black lines) show the excess phase, the excess Doppler shift, the power loss and the bending angle. The excess Doppler shift ranges from 0.11 m/s at 10 km to 1.38 m/s at 0 km. The bending angle increases from 0.24° at 10.3 km to 1.47° at the surface. The power loss at the surface is 6.2 dB.

The expected airplane velocity error using an integrated GPS/Inertial Navigation System (INS) is on the order of 5 mm/s (Lithopoulos, 1999). This error is less than 5% of the signal level at the start of the occultation at 10 km, and less than 0.4% of the signal level at the end of the occultation at 0 km.

Concerning the positioning and velocity error specifications, this accuracy is quoted for systems that use a ground based reference receiver less than 50 km from the airborne receiver. While we note that similar accuracy has been found at distances up to 350 km from a

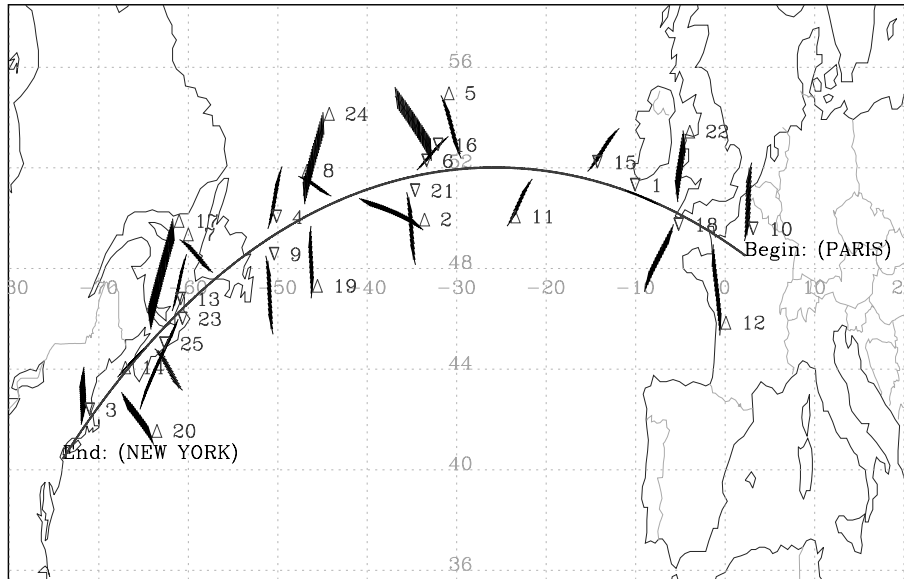


Fig. 2. 25 Occultations generated by EGOPS for a Paris–New York flight. Up-triangles indicate rising events and down-triangles setting events. The profiles, seen in more detail on this figure than Fig. 1, also include hatches which indicate the line of sight for individual ray paths during the occultation.

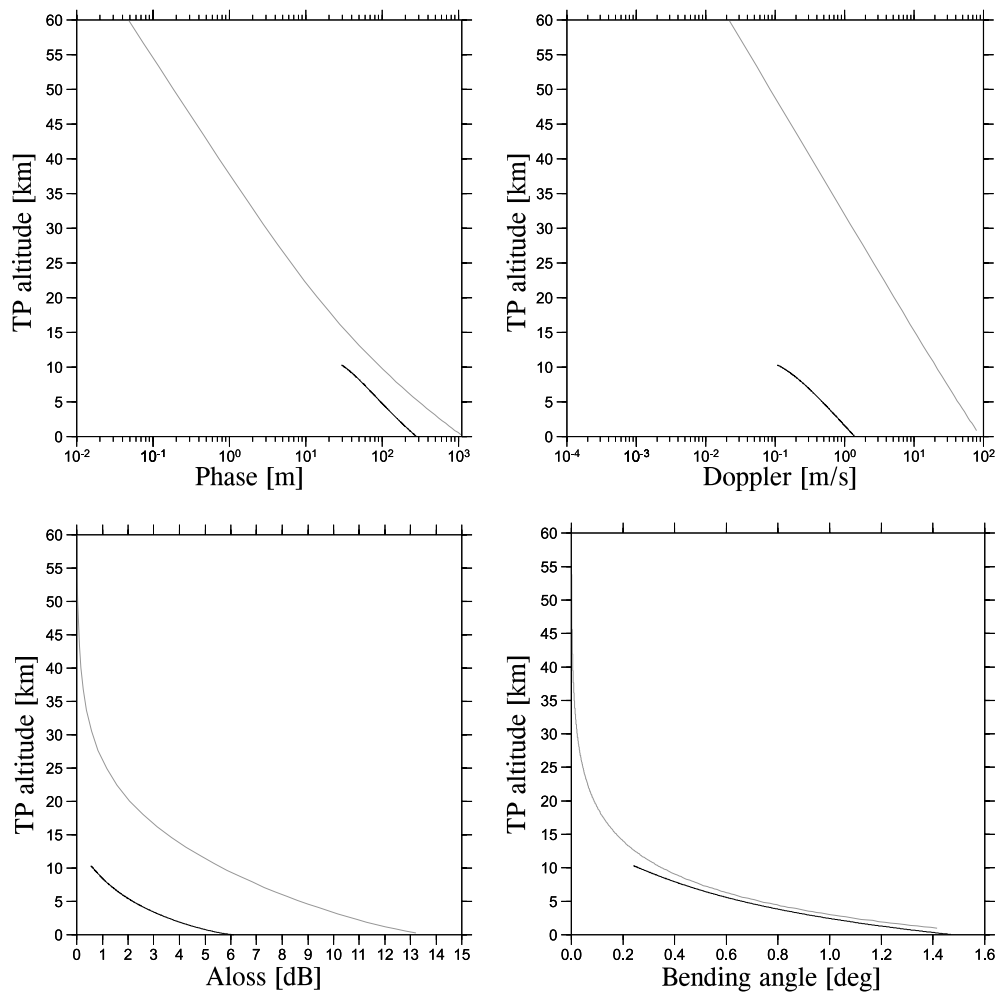


Fig. 3. Vertical profiles of excess phase, power loss, excess Doppler shift and bending angle as a function of tangent point altitude (TP): airplane case (black) and LEO case (grey) with the same topmost tangent point as that of the airborne case.

reference station (IFP Stuttgart, 2001) there is still a technical challenge for achieving this accuracy for transatlantic flights.

3.2. Comparison with the LEO case

We extracted the coordinates of the topmost tangent point (50.8°N, −35.4°W) as well as the occultation plane azimuth (N 169°) of the airborne reference occultation in order to simulate an equivalent occultation geometry for the LEO case over an altitude range from 0 to 60 km. The simulation supposes an idealized geometry in which the source and receiver move away from each other in a plane coincident with the line of sight, which allows the EGOPS user to specify precisely the location of the tangent point of the profile. We once again used the bi-exponential atmospheric model and no ionosphere. Fig. 3 (lines in grey) shows the results for this case.

In this LEO case, the occultation duration is much shorter than in the airplane case, taking only 38 s, the last 19 s of which cover the part of the profile from 10 km to the surface. During this time, the tangent point has drifted by only ~60 km as it passed from an altitude of 60–0 km, and only 46 km in the lowest 10 km. The excess phase increases from 0 to 1067 m, reaching a level approximately four times greater than the excess phase in the airplane case. Concerning the Doppler shift, it varies from 0.05 m/s at 60 km to 79.9 m/s at 0 km. The bending angle in the LEO case increases from $\sim 3 \times 10^{-4}^\circ$ at 60 km to 1.42° at the surface.

The power loss reaches 13.2 dB after 38 s (at 0.3 km), which is 7 dB greater than in the airplane case, because of the additional travel path towards the LEO. The fact that the aircraft occultation only suffers about 6 dB atmospheric loss is a significant advantage of the airborne system over the spaceborne system for sounding the lower troposphere, particularly since the profiles from the GPS/MET mission frequently stopped above 5 km due to low signal to noise ratio (Rocken et al., 1997). We should note, though, that the first results of the recently started CHAMP/GPS mission (Wickert et al., 2001) show that the majority of spaceborne profiles reach close to the surface now, due to spaceborne receiver and antennae advancements achieved since the time of GPS/MET.

4. Phase and Doppler sensitivity to refractivity changes

The objective of these simulations is to make first-order estimates of the relative effects of some instrumental error sources, namely airplane position and velocity uncertainty, on refractivity using forward modeling of refractivity perturbations to a reference atmosphere.

In order to introduce a perturbation to the refractivity structure at a given height without violating the hydrostatic equilibrium condition, we used a Gaussian perturbation as described by (Hoeg et al., 1995) for modeling tropopause disturbances. The perturbation is limited in width to a minimum of 2 km.

4.1. Phase sensitivity to refractivity changes

We introduced a disturbance of a given amplitude on a bi-exponential background profile at an altitude of 3 km. We then compared the phase profile obtained for the reference model with that obtained with the perturbed model. The difference in phase is shown in the first panel of Fig. 4. EGOPS produces phase profiles as a function of time. In order to compare the phase for the same ray path through the atmosphere, we first had to extract the tangent point corresponding to each phase observation for the two simulations. Then the phase was differenced for two ray paths with the same tangent point altitude. We repeated this calculation for a range of percentage refractivity perturbations from 0.2% to 3.0%. In each case the Gaussian disturbance has a width of 2 km. The other panels of Fig. 4 show the same calculation for input disturbances at a range of altitudes from 4 to 10 km. The decrease in the maximum peak as a function of altitude demonstrates the decrease in sensitivity of the measurements to the refractivity perturbation.

The left panel of Fig. 5 summarizes all the plots from Fig. 4. We have derived a reference, which shows for a given refractivity perturbation the resulting effect on the phase observations as a function of tangent point altitude. From this figure we can extract the information that for aircraft position errors on the order of 10 cm, refractivity differences on the order of 1% over a scale length of 2 km are visible above the noise at the altitude of the airplane (near 11 km), refractivity differences on the order of 0.5% over a scale length of 2 km are well visible above the noise at a height of 7 km, and refractivity differences on the order of 0.2% over a scale length of 2 km are above the noise level at a height of 3 km.

Fig. 5 (right panel) exhibits this information from another perspective, now showing for a set of given altitudes what the expected refractivity accuracy as a function of the phase error is (due to the position uncertainty of the aircraft). We emphasize that the phase errors considered here are not the precision of the phase measurements of the receiver, which in general are on the order of 100th of a wavelength or 0.3 mm (Kleusberg and Teunissen, 1996). The limiting error is the phase error introduced into the excess phase due to the uncertainties in the aircraft position, which is itself derived from phase measurements to non-occluding GNSS satellites. In this case we are most concerned with the

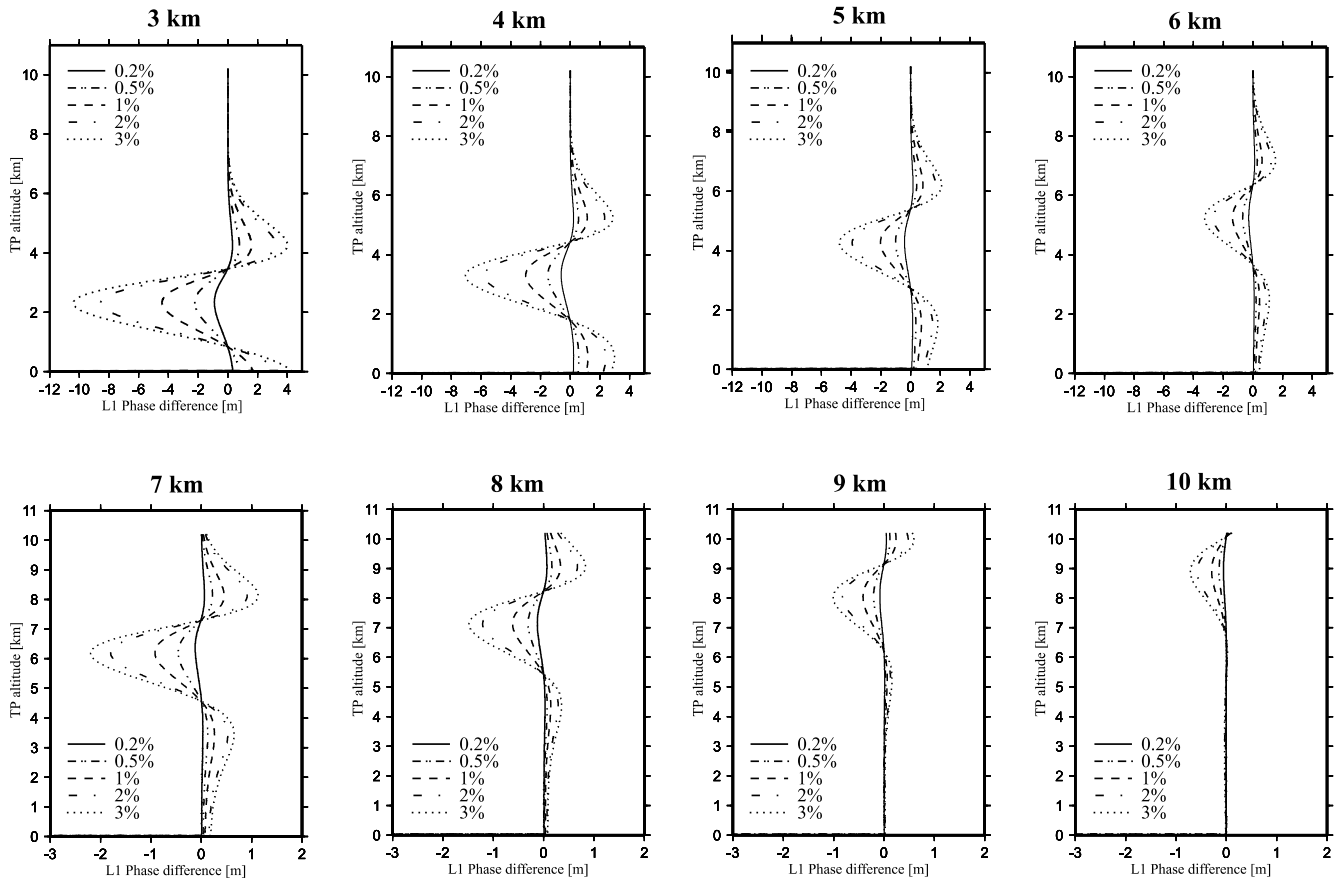


Fig. 4. Phase difference (phase of forward models with refractivity perturbation minus phase of the reference model) as a function of tangent point altitude for refractivity perturbations from 3 to 12 km using the tropopause disturbance model of EGOPS.

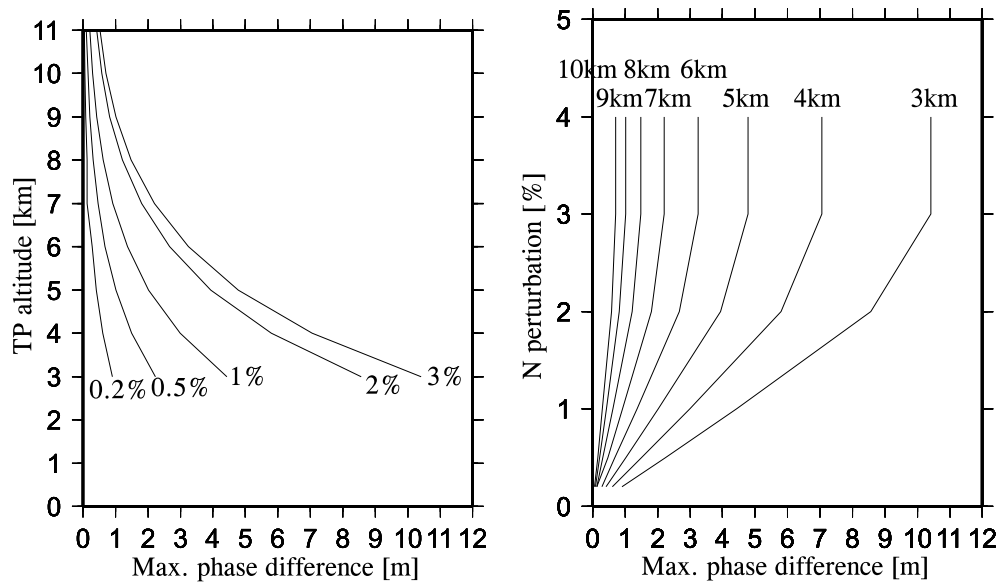


Fig. 5. Maximum phase difference corresponding to different percentage refractivity perturbations as a function of tangent point altitude (left panel) and corresponding to different tangent point altitudes as a function of percentage refractivity perturbation (right panel).

horizontal positioning accuracy because the line of sight is nearly horizontal. Fortunately, phase needs to be known only up to a constant as only its time derivative, the Doppler shift, is the quantity of primary interest for further retrieval processing.

4.2. Doppler sensitivity to refractivity changes

We have made the same calculation in terms of Doppler, since this is the observation directly entering the bending angle calculation. Once again, we examine the effect of different percentage changes in the refractivity to determine what level of variation gives a Doppler difference on the order of the expected airplane velocity error, which we gave earlier as 5 mm/s for a sampling of up to 200 Hz. The Doppler shift differences (forward model Doppler shift minus reference case Doppler shift) as a function of tangent point altitude are shown in Fig. 6. The phase has been differentiated to produce excess Doppler. The Doppler is less sensitive to this type of long-wavelength refractivity perturbation than the phase observations.

A change of 0.2% in the refractivity gives a maximum Doppler shift difference of only 0.95 mm/s for rays with a tangent point altitude of 7 km. But a change of 1% in refractivity gives a Doppler difference of 4.6 mm/s for rays with a tangent point altitude of 7 km, which is approximately the level of the airplane velocity error. However the change in Doppler is spread out over a time interval of more than 100 s.

From this we can infer that an error of about 5 mm/s in the airplane velocity at an altitude of 7 km should produce a maximum error of not more than 1% in the refractivity profile. This is an extreme upper limit, however, since the velocity error is more realistically represented as a random error sampled at 1 Hz, and the velocity error averaged over a longer time interval will not be as large. In other words, the modeled change in the Doppler occurs over a time scale of 100 s, and the accuracy of the airplane velocity is much better than 5 mm/s over 100 s.

In conclusion, given that the velocity error of the aircraft is approximately 5 mm/s, the measurements should be able to detect refractivity differences at least as

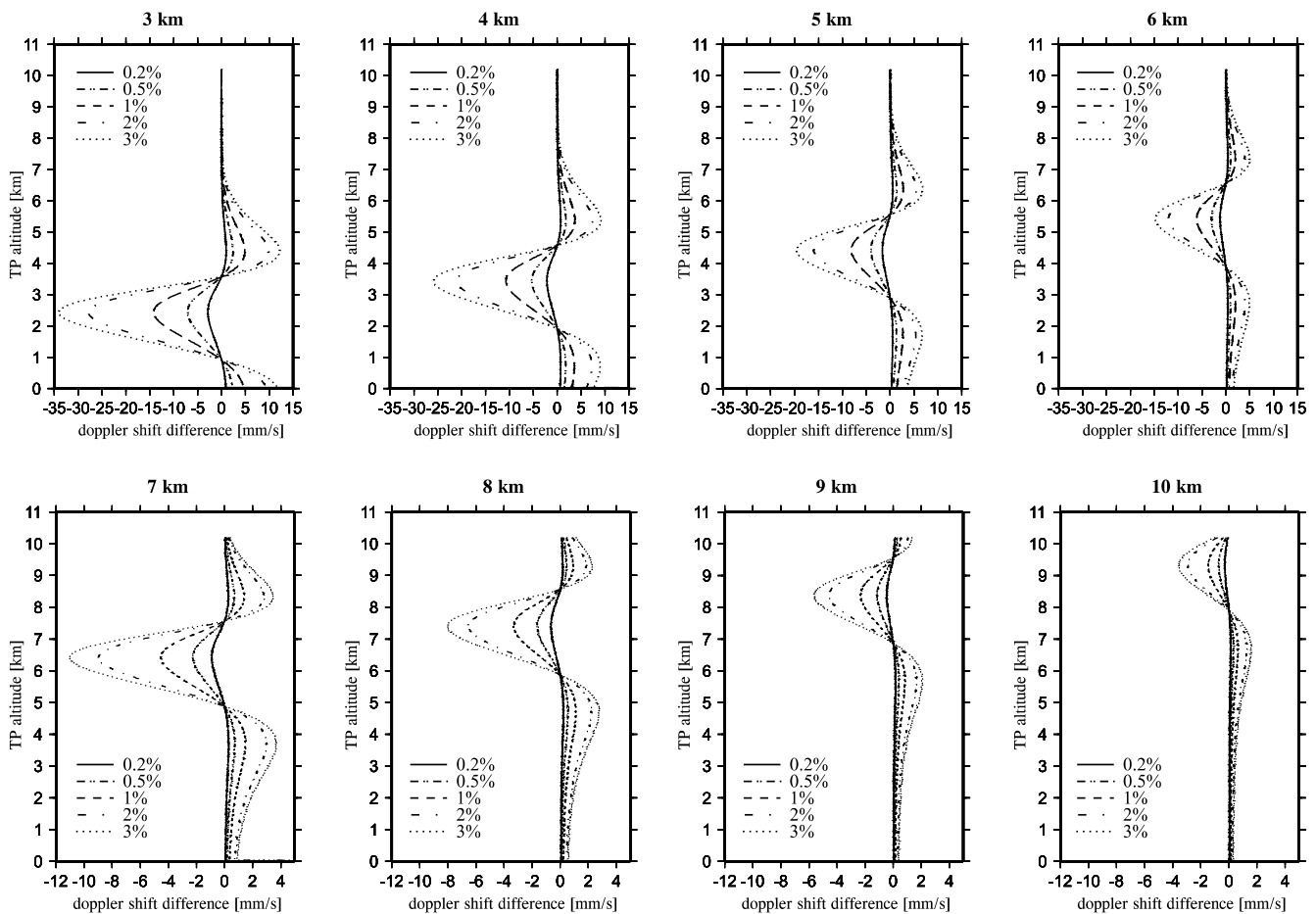


Fig. 6. Doppler shift difference (Doppler shift of forward models with refractivity perturbation minus Doppler shift of the reference model) as a function of tangent point altitude for refractivity perturbations from 3 to 10 km using the tropopause disturbance model of EGOPS.

accurately as 1% at a height of 7 km and with better relative accuracy below.

5. Conclusions

We have simulated the distribution of occultations in order to address the sampling to be expected from an airborne radio occultation system. The simulations take into account realistic characteristics of the transmitter geometries based on the GPS constellation and on realistic characteristics of possible receiver geometry scenarios based on the AMDAR database flight paths. Results show that an airborne system has the potential to provide more profiles below 10 km height, in particular over the North Atlantic covered by many flight trajectories, than LEO systems of 1–25 satellites, though not with global coverage.

Concerning the signal dynamics, for an average profile, the Doppler ranges from 0.11 m/s at 10 km to 1.38 m/s at 0 km. The velocity error for a state-of-the-art commercial receiver positioning system is 0.005 m/s, which is less than 5% of the minimum Doppler shift. Even though the receiver velocity error is larger than for the LEO system, it is thus still small relative to the signal level. The power loss is only about 6 dB compared to about 13 dB for the LEO case, which provides an advantage for sampling in the lower troposphere.

The limiting measurement error sources are the receiver velocity error. For occultations with large tangent point drift, errors due to the spherical symmetry assumption are also expected to be a limitation. Airborne occultations typically show tangent point drifts ranging from 200 to 470 km, significantly larger than spaceborne ones.

A 5 mm/s velocity error contributes about 1% to the refractivity error at altitudes of 7 km and above. This is high frequency noise that seriously degrades the quality of the bending angle data. Assuming that through optimal filtering of the Doppler data this velocity error can be reduced to 1 mm/s, it would be possible to retrieve the refractivity with a better accuracy approaching 0.5% refractivity, satisfying user requirements.

Forward modeling simulations were used to quantify the change in the excess phase observation corresponding to a given refractivity perturbation. Based on these simulations, a position error of 10 cm would give an expected error in refractivity ranging from 0.02% at 3 km to 0.5% at 11 km. This would correspond to an accuracy in retrieved relative humidity, assuming the temperature profile was known from independent data, of about 0.2% at 3 km, 0.6% at 5 km and 7% at 7 km. These results are much more optimistic than the velocity error analysis about the useful information that could be extracted from the data. The difference stems from the fact that the velocity error is assumed to be an instan-

taneous error that affects an individual observation, whereas the forward modeling simulations for the position error assume that we are attempting to resolve features that have 2 km vertical scale length which correspond to an observation error spread over a much longer time period. There is a trade-off between vertical resolution and accuracy that must be optimized. This will be the subject of future study. Future work will also include the derivation of appropriate retrieval algorithms to provide more refined estimates of the accuracy of the retrieved atmospheric parameters.

In general, it seems clear already at this point that airborne occultation data hold significant promise to become a valuable complement to data from global spaceborne occultation observing systems. There is an ambiguity in determining both temperature and humidity from the derived refractivity. Because of the relatively high uncertainties in numerical weather prediction model estimates of humidity compared to uncertainties in temperature in the 0–10 km range that is sensed, the technique will be most useful for contributing to knowledge of the humidity fields. The results show that the method is capable of making sufficiently accurate measurements, however a challenge remains in dealing with lateral variations in refractivity in the inversion process.

Acknowledgements

This work was supported by ESA/ESTEC contract 14384/00/NL/DC. The authors thank Stewart Taylor and the UK Met Office for facilitating access to the AMDAR data.

References

- EUCOS, 1997. The EUCOS (EUMETNET Composite Observing System) Strategy. In: Gerard, F. (Ed.), 4th EUMETNET Council Meeting, Athens, May 1997. EUMETNET, Athens, Greece.
- Fjeldbo, G., Kliore, A.J., Eshleman, V.R., 1971. The Neutral atmosphere of Venus as studied with the Mariner V radio occultation experiments. *Astron. J.* 76 (2), 123–140.
- Hoeg, P., Hauchecorne, A., Kirchengast, G., Syndergaard, S., Belloul, B., Leitinger, R., Rothleitner, W., 1995. Derivation of Atmospheric Properties using a Radio Occultation Technique, ESA Contract Report, ESTEC/C. No. 11024/94/NL/CN, ESA Contract, Danish Met. Institute, Copenhagen, Denmark, 208 pp.
- IFP Stuttgart, 2001. Accuracy of an airborne GPS/INS system for photogrammetry applications, <http://www.ifp.uni-stuttgart.de/ifp/sensor>.
- Kirchengast, G., 1998. End-to-end GNSS occultation performance simulator overview and exemplary applications *Wissenschaftl. Ber.* No. 2/1998, Institute for Meteorology and Geophysics, University of Graz, Graz, Austria, 138 pp.
- Kirchengast, G., Pötzi, W., Ramsauer, J., Steiner, A.K., Syndergaard, S., Gorbunov, M., Larsen, G.B., Schultz, K., Reichinger, H., Silvestrin, P., 2001. EGOPS4 – An end-to-end simulator for

- atmospheric sounding based on GNSS signals. In: European Geophysical Society 26th General Assembly (edited by EGS, EGS, Nice, France).
- Kleusberg, A., Teunissen, P.J.G., 1996. *Lecture Notes in Earth Sciences: GPS for Geodesy*. Springer Verlag, Berlin.
- Lithopoulos, E., 1999. A modular integrated inertial/GPS system for survey and mapping applications. In: *ION GPS 99*. Institute of Navigation, Nashville, TN, pp. 1897–1900 (edited by I.o. Navigation).
- Melbourne, W.G., Davis, E.S., Duncan, C.B., Hajj, G.A., Hardy, K.R., Kursinski, E.R., Meehan, T.K., Young, L.E., Yunck, T.P., 1994. *The Application of Spaceborne GPS to Atmospheric Limb Sounding and Global Change Monitoring*. JPL Publication, Jet Propulsion Laboratory, Pasadena, 147 pp.
- Ramsauer, J., Kirchengast, G., 2000. End-to-end GNSS occultation performance simulator Version 3 (EGOPS3), Software User Manual (SUM). Technical Report for ESA/ESTEC No. 1/2000. Institute for Geophysics, Astrophysics, and Meteorology, University of Graz, Graz, Austria, 467 pp.
- Rocken, C., Anthes, R., Exner, M., Hunt, D., Sokolovskiy, S., Ware, R., Gorbunov, M., Schreiner, W., Feng, D., Herman, B., Kuo, Y.-H., Zou, X., 1997. Analysis and validation of GPS/MET data in the neutral atmosphere. *J. Geophys. Res.* 102, 29849–29866.
- Vorobev, V.V., Krasil'nikova, T.G., 1994. Estimation of the accuracy of the atmospheric refractive index recovery from Doppler shift measurements at frequencies used in the NAVSTAR system. *Phys. Atmos. Ocean* 29 (5), 602–609 (English translation).
- Ware, R., Exner, M., Feng, D., Gorbunov, M., Hardy, K.R., Herman, B.M., Kuo, Y., Meehan, T.K., Melbourne, W.G., Rocken, C., Schreiner, W., Sokolovskiy, S., Solheim, F., Zou, X., Anthes, A., Businger, S., Trenberth, K., 1996. GPS Sounding of the atmosphere from low Earth orbit: preliminary results. *Bull. Am. Meteor. Soc.* 77 (1), 19–40.
- Wickert, J., Reigber, C., Beyerle, G., König, R., Marquardt, C., Schmidt, T., Grunwaldt, L., Galas, R., Meehan, T.K., Melbourne, W.G., Hocke, K., 2001. Atmospheric sounding by GPS radio occultation: first results from CHAMP, *Geophys. Res. Lett.* 28, 3263–3266.
- Zuffada, C., Hajj, G., Kursinski, E.R., 1999. A novel approach to atmospheric profiling with a mountain-based or airborne GPS receiver. *J. Geophys. Res.* 104 (D20), 24435–24447.